July 1999 • NREL/CP-500-26829

Conference Paper

A Case for Including Atmospheric Thermodynamic Variables in Wind Turbine Fatigue Loading Parameter Identification

Neil D. Kelley
National Wind Technology Center

Second Symposium on
Wind Conditions for Wind Turbine Design
IEA Annex XI
Roskilde, Denmark
April 12–13, 1999

National Renewable Energy Laboratory

1617 Cole Boulevard
Golden, Colorado 80401-3393

NREL is a U.S. Department of Energy Laboratory
Operated by Midwest Research Institute • Battelle • Bechtel

Contract No. DE-AC36-98-GO10337

NOTICE

Available to DOE and DOE contractors from:
Office of Scientific and Technical Information (OSTI)
P.O. Box 62
Oak Ridge, TN 37831
Prices available by calling 423-576-8401

Available to the public from:
National Technical Information Service (NTIS)
U.S. Department of Commerce
5285 Port Royal Road
Springfield, VA 22161
703-605-6000 or 800-553-6847
or
DOE Information Bridge
http://www.doe.gov/bridge/home.html

 Printed on paper containing at least 50% wastepaper, including 20% postconsumer waste

IEA Annex XI
2nd Symposium, *Wind Conditions for Turbine Design*
Risø National Laboratory
Roskilde, DK , 12-13 April 1999

A CASE FOR INCLUDING ATMOSPHERIC THERMODYNAMIC VARIABLES IN WIND TURBINE FATIGUE LOADING PARAMETER IDENTIFICATION

N.D. Kelley
National Wind Technology Center
National Renewable Energy Laboratory
Golden, Colorado U.S.A.

ABSTRACT

This paper makes the case for establishing efficient predictor variables for atmospheric thermodynamics that can be used to statistically correlate the fatigue accumulation seen on wind turbines. Recently, two approaches to this issue have been reported. One uses multiple linear-regression analysis to establish the relative causality between a number of predictors related to the turbulent inflow and turbine loads. The other approach, using many of the same predictors, applies the technique of principal component analysis. An examination of the ensemble of predictor variables revealed that they were all kinematic in nature; i.e., they were only related to the description of the velocity field. Boundary-layer turbulence dynamics depends upon a description of the thermal field and its interaction with the velocity distribution. We used a series of measurements taken within a multi-row wind farm to demonstrate the need to include atmospheric thermodynamic variables as well as velocity-related ones in the search for efficient turbulence loading predictors in various turbine-operating environments. Our results show that a combination of vertical stability and hub-height mean shearing stress variables meet this need over a period of 10 minutes.

INTRODUCTION

A recent study has recently identified and modeled the dominant inflow turbulence-scaling parameters responsible for the accumulation of fatigue in wind turbines operating in complex terrain environments. Called MONTURB, this international, multi-laboratory effort analyzed measurements of both the inflow turbulence and wind turbine dynamic variables for several turbines in both relatively smooth and complex terrain sites in Greece, Denmark, Spain, and the United States (California) [1,2,3]. Using sensitivity

analysis, analysts concluded that the fatigue loads increased significantly with the standard deviation of the longitudinal wind speed (σ_u), which was also considered as the primary fatigue driver. One part of the MONTURB study [4], which was incorporated in [2], applied multivariate regression to analyze the statistical response of turbine fatigue loads to a wide range of turbulence descriptors (including higher order statistical moments). These analyses were based on data from a substantial array of turbulence and load measurements taken for a single turbine installed at the crest of a hill in Greece. A similar study conducted in Spain used principal component analysis to examine the effect of several turbulence descriptor variables on fatigue-load factors [5].

The turbulence descriptors used as explanatory or predictor variables in [2, 4] included the following

- Mean wind speed (U)
- Power law wind-shear exponent (α)
- Inclination angle between the wind vector and the horizontal (ψ)
- Standard deviations of the longitudinal, lateral, and vertical wind components (σ_u, σ_v, and σ_w)
- Longitudinal, lateral, and vertical turbulence length scales (L_u, L_v, and L_w)
- Skewness of U [$\sigma_3(U)$]
- Kurtosis of U [$\sigma_4(U)$]
- Davenport decay factor between two elevations (A_{z1} and A_{z2})
- Ratios σ_v/σ_u and σ_w/σ_u.

The cross-correlation of the longitudinal and vertical wind components (ρ_{uw}) and the U, σ_u, $\sigma_3(U)$, $\sigma_4(U)$, σ_v/σ_u, and σ_w/σ_u parameters was used by [5].

In both studies, the response variable chosen was the equivalent load parameter defined by

$$\text{Equivalent Load} = L_{eq} = \left(\frac{\sum n_i L_i^m}{N_{eq}} \right)^{\frac{1}{m}}$$

where n_i is the number of cycles in the i^{th} load range, L_i is the maximum (conservative) value of each load level in a bin, N_{eq} is the equivalent number of constant-amplitude cycles, and m is the slope of the material S-N curve. For these studies, record lengths of 10 minutes were used and a 1-Hz equivalent load calculated, which set N_{eq} to 1200 half-cycles for that period. The effect of various materials was evaluated by applying S-N curve slopes in the range of 4 to 12. Using this definition, L_{eq} repeated N_{eq} times is equivalent to the same fatigue damage contained in the measured load spectrum [2].

A review of the above-mentioned turbulence descriptors used as predictor variables results in the realization that they are all *kinematic*; i.e., they are all related to the description of the inflow *velocity* field. In 1994, we reported on the results of a similar experiment involving the 10-minute load response of two side-by-side wind turbines deep within a multi-row wind farm in San Gorgonio Pass, California [6]. We also applied multivariate regression and the analysis of variance (ANOVA) to assess the sensitivity of a range of turbulence descriptors on the measured loading spectra. Our predictor variable list, although including many of the variables listed above, also contained the following kinematic variables and their higher moments measured at hub height:

- Mean *horizontal* wind speed, defined by $U_H = \sqrt{U^2 + V^2}$
- Standard deviation of U_H (σ_H)
- Turbulence intensity (σ_H/U_H)
- Mean longitudinal, lateral, and vertical wind components aligned with the mean shear vector (U, V, and W)
- Reynolds stress components (u'w', u'v', and v'w') where u', v', and w' are the zero-mean, fluctuating components of U, V, and W
- Local friction velocity, defined by $u_* = \sqrt{\left|\overline{u'w'}\right|}$
- Cross-correlation coefficients of u'w', u'v', and v'w' ($\rho_{u'w'}$, $\rho_{u'v'}$, $\rho_{v'w'}$)
- Standard deviations of the instantaneous Reynolds stresses ($\sigma_{u'w'}$, $\sigma_{u'v'}$, $\sigma_{v'w'}$)
- Skewness coefficients of instantaneous values of u'w', u'v', and v'w' [$\sigma_3(u'w')$, $\sigma_3(u'v')$, $\sigma_3(v'w')$]
- Kurtosis coefficients of instantaneous values of u'w', u'v', and v'w' [$\sigma_4(u'w')$, $\sigma_4(u'v')$, $\sigma_4(v'w')$].

In addition to the kinematic variables and their derivations listed above, we also included the following parameters that are related to the *thermodynamics* of the planetary boundary layer:

- turbine-layer gradient Richardson number (Ri) stability parameter defined by

$$Ri = \left(g/\overline{\theta}_m\right)\left[\left(\partial\overline{\theta}/\partial z\right)\Big/\left(\partial\overline{U}/\partial z\right)^2\right]$$

  where g is the gravity acceleration, z is the height in meters, θ_m is the layer mean thermodynamic potential temperature (K) given by $\theta(z) = T(z)[1000/p(z)]^{0.286}$, and T(z) and p(z) are the temperature (K) and barometric pressure (hPa), respectively at height z. The turbine layer is defined as the

vertical distance between the surface and the maximum elevation of the wind turbine rotor. The over bars represent 10-minute averages.

- Hub potential temperature (θ_{hub})
- Cross-correlation coefficient of $w'\theta_{hub}'$ ($\rho_{w'\theta'}$)
- $w'\theta'$ covariance or vertical temperature flux ($\overline{w'\theta_{hub}'}$)
- Standard deviation, skewness, and kurtosis of $\overline{w'\theta_{hub}'}$.

The response variable we used for most load parameters, except edgewise bending, was the slope (β_1) of the high-loading tail or low-cycle, high-amplitude portion of the loading spectral distribution. This tail region is a major contributor to the fatigue damage seen in materials with large S-N slopes. The loading spectral tails are fitted with an exponential distribution $N = -\beta_o e^{-\beta_1 M_{p-p}}$, where M is the peak-to-peak or alternating load range and N is the number of cycles.

We also found that the slope β_1 was most sensitive to the atmospheric stability expressed by the turbine layer Ri and the u'w'-component of the Reynolds stress or its square root, u_*. We observed that the slope varied indirectly with u_* and Ri; e.g., higher values of u_* and/or Ri produced a shallower slope and higher potential fatigue damage and vice versa. These results indicated that, at the minimum, *both* a kinematic and a thermodynamic turbulence-related descriptor are necessary for a linear, multivariate regression model that can explain a high percentage of the observed variance. Finally, we found that more than 89% of the observed variance of the combined turbine flapwise loads could thus be explained.

A CASE STUDY WITHIN A LARGE, MULTI-ROW WIND FARM

In 1990, the National Renewable Energy Laboratory (NREL) operated two adjacent Micon 65/13 wind turbines deep within a very large wind farm in San Gorgonio Pass, California. Both of the turbines were identical except that one used a rotor based on the NREL 7.9m Thin Airfoil Family; the other was an original AeroStar design. We will refer to the turbine using the NREL blades as *Rotor 1* and the AeroStar-equipped turbine as *Rotor 2*. A total of 397 10-minute records were taken over a wide range of inflow conditions during late July and August, the latter half of the San Gorgonio wind season.

Inflow measurements for the turbines were taken using a near-hub-height (21-m), three-axis sonic anemometer/thermometer and propeller-vane anemometers installed at three elevations. Temperature,

vertical temperature difference, and the barometric pressure were also recorded. The maximum height of the rotors was 31 meters above ground and the turbine hubs were located at 23 meters. The two test turbines were located downwind, with respect to the prevailing wind direction, about mid-row in Row 37 of a 41-row wind farm that included nearly 1000 machines. The nearest rows of turbines were located approximately seven rotor diameters up and downwind. Although the terrain surrounding the farm was complex (there is a 3700-m mountain peak immediately to the south), locally it is relatively flat desert with a slight upgrade towards the prevailing wind direction. The dominant flow comes through the throat of the mountain pass to the west. However, once or twice during the night, much of the wind farm (including Row 37) is influenced by cool, unstable gravity or drainage flows. These flows, which originate in the high, cold elevations of the mountains to the south spill out onto the desert floor after being funneled down through steep canyons. Intense turbulent bursts are often observed with these drainage winds when they merge and interact with the flow being channeled through the pass to the west. A result of this merger is higher than normal maintenance on the wind turbines that operate in the region of their confluence.

Stability Sensitivities

We calculated the 1-Hz equivalent loads (L_{eq}) from each of the blade-root flapwise rainflow load spectra for each of the three blades of each turbine for S-N slopes of 4, 6, 8, 10, and 12. We then summarized the L_{eq} loads from the three blades and determined the peaks and averages for each turbine. Next, we plotted the three-blade peak and average 1-Hz L_{eq} loads for each rotor and S-N slope parameter m as a function of the turbine-layer gradient Richardson number stability parameter, Ri (see Figure 1). The Richardson number parameter indicates the ratio between turbulence production due to buoyancy and turbulence production caused by wind shear. Negative values represent unstable flow conditions, zero neutral, and positive stable. Unstable flows are characterized by large eddies with a positively buoyant circulation and turbulence energy peaks occurring at large wavelengths. The turbulence in truly neutral flows is generated solely by the action of wind shear and is usually associated with strong winds. Flows with just slightly positive Ri values are often referred to as weakly stable. Under such conditions, the influence of negative buoyancy can produce intense, transient shears at moderate to high wind speeds that are often characterized by bursts of temporally and spatially coherent turbulence whose peak energy is at small wavelengths. As Ri approaches the critical value of 0.25, increased buoyant damping decreases the turbulence levels, eventually reaching more or less laminar conditions at 0.25 and above.

The graphs of Figure 1 clearly distinguish a structural change in the load characteristics as the stability transitions from unstable to stable. The largest loads for all values of the S-N slope parameter occur in the weakly stable region. Furthermore, as the value of the S-N slope parameter increases, the fatigue damage also increases in this stability region. A distinct cluster of high-level peak L_{eq} loads develops for values of m=10 and m=12 in the Ri range of approximately –0.01 to +0.10. This suggests that under such conditions, rotor blades made of materials such as glass fiber and exhibiting high values of S-N slopes will sustain greater fatigue damage.

This increased damage can be further substantiated by noting that the cluster of peak L_{eq} loads for m=10 and m=12 in Figure 1 occur at values exceeding 20 kNm. We determined that there are 16 10-minute records contained within this cluster, whose associated mean wind speed ranged from 12.25 to 15.09 m/s. Excluding the elements of this cluster, we searched the remaining database for records whose mean wind speeds fell within this range. We found that there were 49 records of the remaining 381 available that met this criteria. We then summarized the individual load spectra associated with the records of the peak cluster and 49 other records from both turbine rotors into two composite spectra. Best-fit curves were regressed through each of these spectra and the results plotted as a function of cycles per hour (see Figure 2). These curves indicate why the L_{eq} peaks with high values of the S-N slope parameter occurred. The inflow conditions associated with these 16 records contained elements that produced a greater number of high-amplitude cycles than were characteristic of the other 49 records measured within the same wind speed range. Because Figure 1 indicates a strong dependency on the Richardson number, we plotted the distributions of this parameter for each of the above cases in Figure 3. This figure shows that the L_{eq} distribution associated with the high-damage cluster tends to be narrow and uni-modal. It is centered between 21 and 22 h, with the bulk of the occurrences in the range of 20 to 22 h. The L_{eq} distribution of the 49 records with lower peaks is much broader and bi-modal and is centered between 22 and 23 h with peaks at 21 and 01 h. Therefore, the higher fatigue damage for materials with high S-N slopes occurred earlier in the *transition* from the daytime to the nocturnal boundary layer structure. Such damage is therefore strongly *diurnally related*.

Sensitivity to Hub-Height Friction Velocity, u_*

The other parameter that we identified in our earlier work [6] as an efficient predictor of low-cycle turbine load behavior was the hub-height friction velocity, or u_*. Figure 4 presents the variation of the three-blade averaged L_{eq} loads for m=12 for each rotor and the corresponding hub-height u_* values as a function of the turbine-layer Richardson number. Again, there is an abrupt change in both the L_{eq} loads

on the rotors and u_* as the stability transitions from unstable to stable. The high u_* and L_{eq} load regime continues until an Ri value of approximately +0.10 is reached, whereas much lower values are evident in the Ri down to −0.10. Thus, for the operating environment in this particular site, the number of operating hours within a critical Ri range of 0 to +0.10 will see increased fatigue damage, particularly for blades made of high S-N exponent material. This is consistent with the findings of a study by Sutherland and Kelley [7], who compared the measured load spectrum from Rotor 1 with the WISPER spectrum [8]. They found that the San Gorgonio load spectrum contains many more cycles than the WISPER spectrum, and that the increased number of cycles results in more damage. The higher loads and damage at San Gorgonio are attributed to a combination of boundary-layer flows interacting with the complex terrain and upstream turbine wakes.

Distributions of Richardson number and u* at Other Locations at this Site

In 1989 we made extensive turbulence measurements from two 50-meter towers located upwind of Row 1 and downwind of the last turbines of Row 41 using similar but more sensitive instrumentation. The total records from each location are much more extensive than those that were available from Row 37 in 1990. The majority of the measurements were made earlier in the wind season, covering a six-week period approximately from early June to mid July that was characterized by periods of strong winds. There were no turbines upwind of Row 1 and the closest operating row to Row 41 was approximately 14 rotor diameters (D) upstream. In Figures 5a and 5b we compared the distributions of the gradient Richardson number and the hub-height u_* for the upstream, downstream, and Row 37 locations. respectively in Figures 5a and 5b. Figure 5a shows the predominance of operation in the weakly stable region for both the upwind (Row 1) and downwind locations. There is a small, secondary peak at the downwind station and 14-D spacing that coincides with the primary peak at Row 37. In general, the Ri distribution at Row 37 peaks at a slightly more stable value and is much broader than the distributions at the other two locations in the stable region. In comparison with the other two layers, the shallower depth of the Ri measurement layer at Row 37 may have more influence than the other two. The impact of the presence of upstream turbine wakes is clearly visible in the u_* distributions. The median value for the upwind location is 0.771 m/s, 1.106 m/s downwind of Row 41, and 1.161 m/s for Row 37, with the tail reaching values in excess of 1.800 m/s. Thus, from the Ri and u_* distributions shown in Figures 5a and 5b, one would expect the highest fatigue damage at Row 37 and the least from the turbines installed in Row 1. This scenario is essentially what the wind farm operator has observed.

DIURNAL VARIATION AS AN IMPORTANT PARAMETER

One of most sensitive factors affecting thermodynamic-related turbulence descriptors is the time-of-day (or diurnal) variation (see Figure 3). The daily heating and cooling cycle of the earth's boundary layer is a major source of variation. This is true in most locations except, of course, in arctic regions during periods with little or no sunlight reaching the usually snow covered surface. Even here thermodynamics may still be important, because very strong inversions often exist with much warmer air aloft that is occasionally brought to the surface through some form of intrusion process. The diurnal heating and cooling of complex terrain features is known to alter the flow characteristics around such obstacles.

In Figure 6 we plotted the diurnal variation of the three-blade average 1-Hz L_{eq} loads using m=12 for each of the two rotors in the San Gorgonio wind farm. The shaded region between 20 and 22 h corresponds to the period where the majority of the peak loads were observed, as discussed earlier. The distribution of L_{eq} loads is strongly diurnal and follows the hourly variation in mean wind speed. This profile is largely controlled by the large-scale dynamics of the region, which are modulated by the complex terrain features (i.e., the mountains and the pass). The strongest winds tend to occur two or three hours after local sunset when the boundary layer is in the process of transitioning from the day to night boundary layer structure. Between 10 and 15 h the wind generally drops below power generation levels as (see Figure 6).

The diurnal relationship between the thermal field and the hub-height mean shearing stress or u_* is shown in Figure 7. We plotted the variation of u_* (dotted circles) and the covariance of the fluctuating vertical velocity component and potential temperature, which is the vertical temperature flux (filled triangles). A positive temperature flux indicates that heat is being transported away from the surface. The period of sunrise is clearly visible between 06 and 08 h with a strong, positive temperature flux readily evident. Local sunset is between about 19 and 20 h on this diagram. At approximately 19 h the vertical temperature flux reaches a maximum for the day, at the same time the sun is setting. This indicates the presence of a strong, positive, vertical velocity field transporting a net heat flow into the boundary layer. Immediately after this peak, the u_* increases rapidly as the temperature flux falls at more or less the same rate. It is during this approximately one-hour period that turbulence production changes from one dominated by buoyant plumes to shear production. Very intense, transient coherent turbulent structures exist in regions of strong vertical velocity fields and rapidly changing shears.

The processes described here are further documented by the diurnal variation of the Richardson number and u_* plotted in Figure 8. Again, the transitions at sunrise and sunset are well characterized by the Ri

and u_* variations. The strong vertical temperature (heat) flux after sunrise quickly destabilizes the boundary layer through positive buoyancy while the shear (u_*) contribution falls, resulting in large negative Ri values. At sunset the inverse occurs with an increasingly stabilizing boundary layer and an increase in the shear which causes the value of Ri to become slightly positive. After about 21 h, the shear becomes the dominant turbulence source damped by a small amount of negative buoyancy, as indicated by the small positive values of Ri. Early in the morning after about 02 h, the Ri begins to rise and the turbulence becomes further damped as the wind speed and shearing stress decrease before reaching a minimum just before sunrise. The diurnal variation of the 1-Hz L_{eq} loads shown in Figure 6 closely mirrors the variation of Ri and u_* of Figure 8; i.e., a combination of negative Ri and low u_* values leads to low L_{eq}. Conversely, during the day-night transition when u_* is high and the Ri weakly positive, the L_{eq} are high and damaging. The variations in the velocity and thermodynamic fields of Figure 7 show why it is necessary to consider both when assessing the efficiency of turbulent load predictor variables.

The processes discussed above are quantified by the turbulent kinetic-energy budget equation given by Panofsky and Dutton [9]:

$$\frac{D\overline{E}}{Dt} = \frac{\partial \overline{E}}{\partial t} = -\left(\overline{u'w'}\right)\left(\frac{\partial \overline{u}}{\partial z}\right) + \frac{g}{\overline{\theta}}\left(\overline{w'\theta'}\right) - \frac{\partial}{\partial z}\left(\overline{Ew'}\right) - \varepsilon = u_*^2\left(\frac{\partial \overline{u}}{\partial z}\right) + \frac{g}{\overline{\theta}}\left(\overline{w'\theta'}\right) - \frac{\partial}{\partial z}\left(Ew'\right) - \varepsilon$$

I **II** **III** **I** **II** **III**

In this equation, the pressure correction term and the effects of moisture were ignored. E is the total kinetic energy given by $E = (1/2)\,(u'^2 + v'^2 + w'^2)$ and ε is the dissipation rate of turbulent kinetic energy. The first term (**I**) of the terms on the right is the shear production term and is always positive. The second term (**II**) is the buoyancy production term and may be positive or negative depending on the sign of the vertical temperature flux $\overline{w'\theta'}$. The values of $\overline{w'\theta'}$ shown in Figure 7 never go negative because of the high surface temperatures in July and August. The third term (**III**) defines the rate at which turbulence is transported into or out of the local volume by velocity fluctuations. This equation couples the importance of the velocity and thermodynamic fields and the related scaling quantities. In a wind farm environment, the third term on the right may be very important due to the transport of upwind turbine wakes.

CONCLUSIONS

In this paper we have underscored the need to include atmospheric thermodynamic variables, such as a measure of vertical stability, when identifying efficient predictors for evaluating turbulence-induced wind

turbine loads. We also have demonstrated that the diurnal variation of these predictors needs to be established for particular site environments or classes of environments. In the United States these classes could include, for example, characteristic Great Plains, mountain passes, elevated ridges, and seashore sites. All exhibit varying degrees of terrain complexity and the large-scale dynamics defining the local wind regime can be quite different from location to location. It is also quite important that the turbulence simulations used in numerical simulations of wind turbine dynamics reproduce the characteristics as discussed here in order to fully appreciate the structural and fatigue impacts of such environments.

ACKNOWLEDGEMENTS

This work has been supported by the U.S. Department of Energy, Contract No. DE-AC36-83CH10093.

REFERENCES

1. Mousakis, F., Morfiadakis, E., and Fragoulis, A. (eds.), November 1996, "MONTURB (JOU2-CT93-0378) Final Report – Volume I," Centre for Renewable Energy Sources, Pikermi, Greece, 182p.

2. Mousakis, F., Morfiadakis, E., and Fragoulis, A. (eds.), November 1996, "MONTURB (JOU2-CT93-0378) Final Report – Volume II," Centre for Renewable Energy Sources, Pikermi, Greece, 245p.

3. Mousakis, F., Morfiadakis, E., and Fragoulis, A. (eds.), November 1996, "MONTURB (JOU2-CT93-0378) Final Report – Volume III," Centre for Renewable Energy Sources, Pikermi, Greece, 42p.

4. Mousakis, F., Morfiadakis, E., and Dellaportas, P., 1996, "Parameter Identification of Fatigue Loading of a Wind Turbine Operating in Complex Terrain," CRES.WE.MNTRB.14, Centre for Renewable Energy Sources, Pikermi, Greece.

5. Cuerva-Tejero, A., López-Diez, S., and Bercebal-Weber, D., 1999, " Higher Level Descriptions of Sites and Wind Turbines by Means of Principal Component Analysis," *Proc. EWECS 1999*, Nice, France.

6. Kelley, N.D., 1994, "The Identification of Inflow Fluid Dynamics Parameters That Can Be Used To Scale Fatigue Loading Spectra of Wind Turbine Spectral Components," NREL/TP-442-6008, National Renewable Energy Laboratory, Golden, CO.

7. Sutherland, H.J. and Kelley, N.D., 1995, "Fatigue Damage Estimate Comparisons for Northern Europe and U.S. Wind Farm Loading Environments," *Proc. WindPower '95*, American Wind Energy Association, Washington, DC.

8. Ten Have, A.A., 1992, "WISPER and WISPERX: Final Definition of Two Standardized Fatigue Loading Sequences for Wind Turbine Blades," NLR-TP-91476U, National Aerospace Laboratory NLR, Amsterdam, The Netherlands.

9. Panofsky, H.A. and Dutton, J.A., 1984, *Atmospheric Turbulence*, Wiley-Interscience, New York, NY, p. 92.

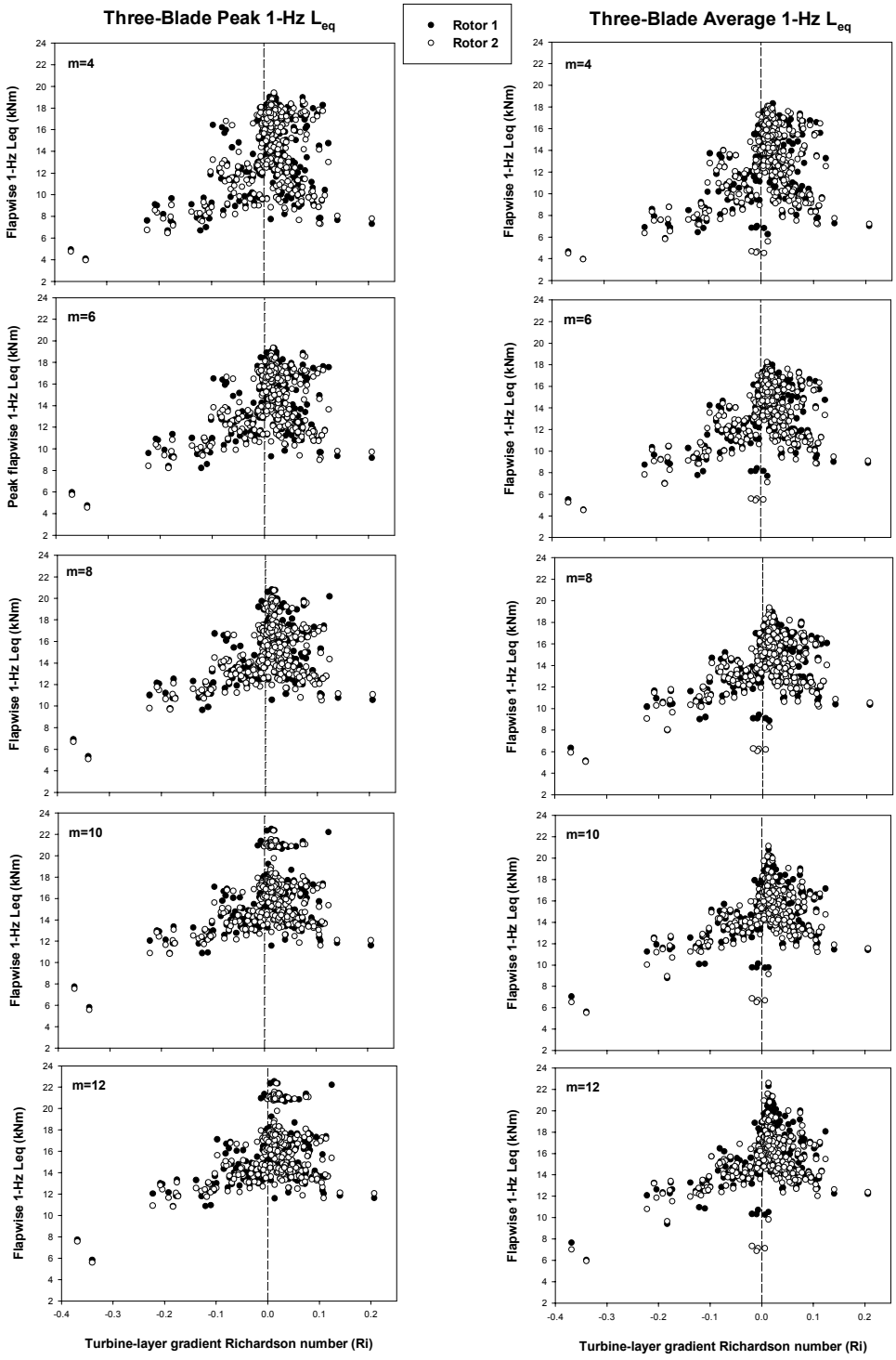

Figure 1. Variation of three-blade peak and average 1-Hz L_{eq} loads with the Richardson number stability parameter

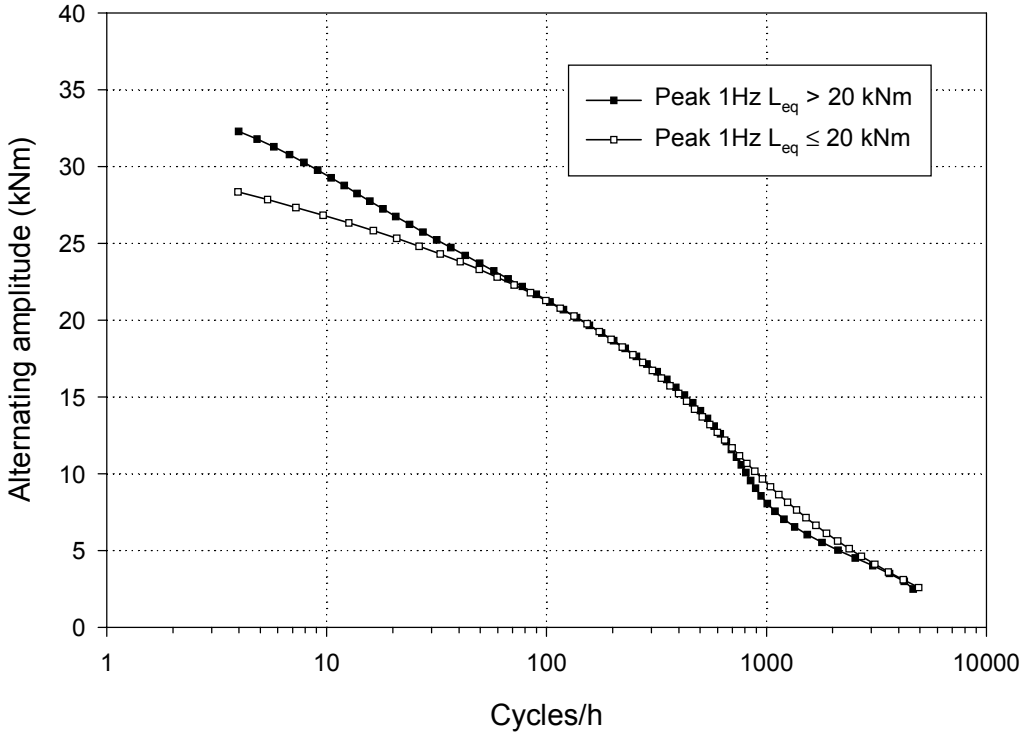

Figure 2. Comparison of peak load cases

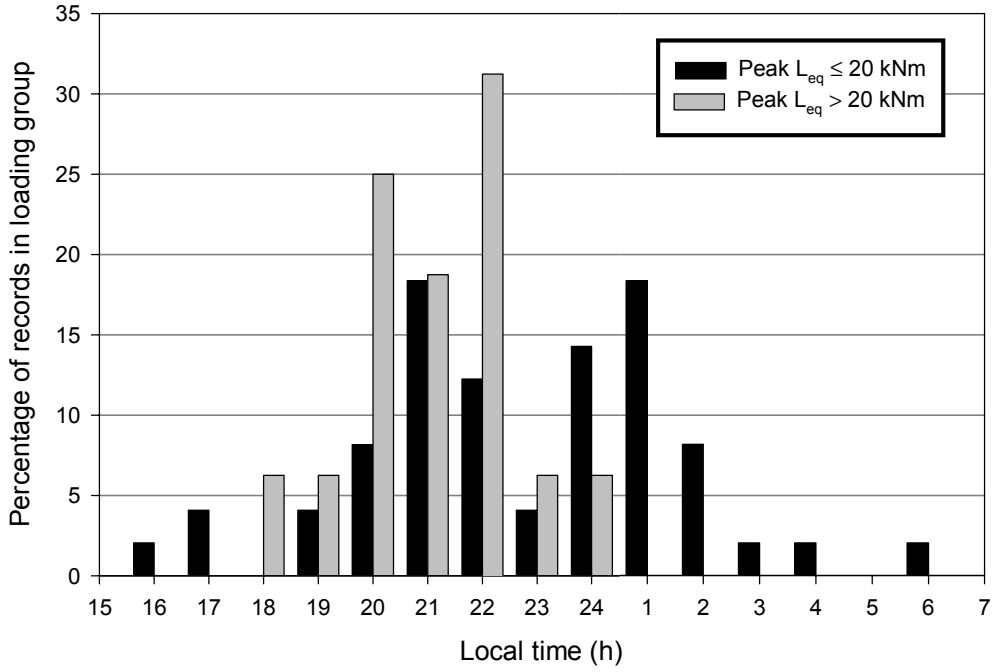

Figure 3. Time distributions of peak loading groups

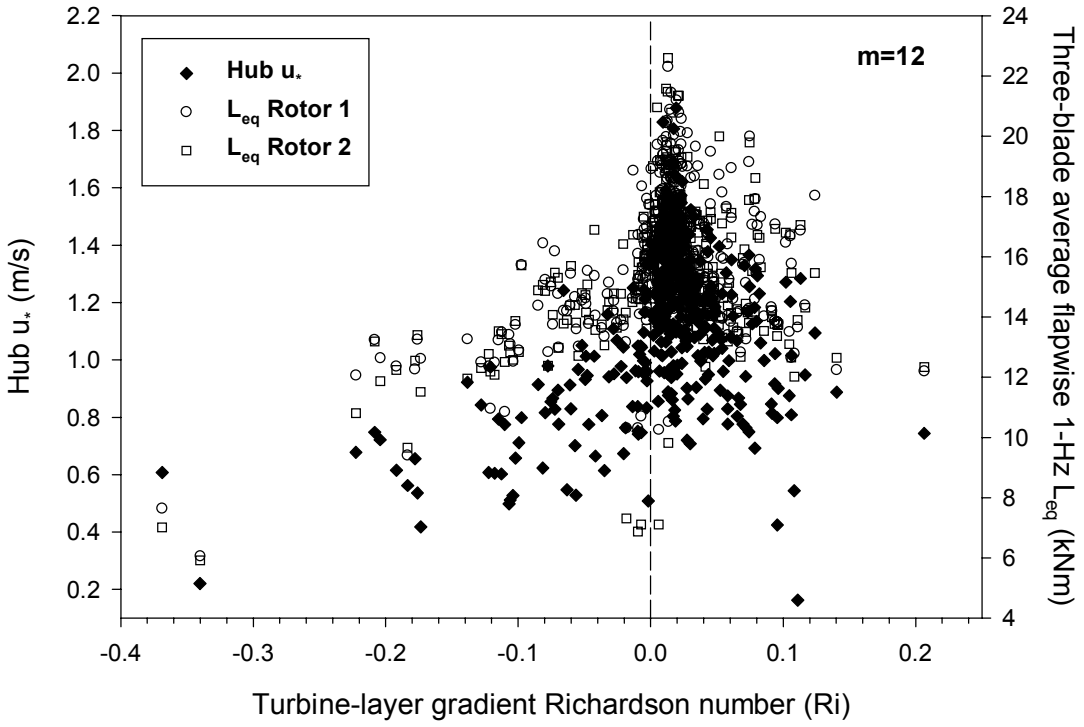

Figure 4. Variation of hub u_* and average 1-Hz L_{eq} with stability

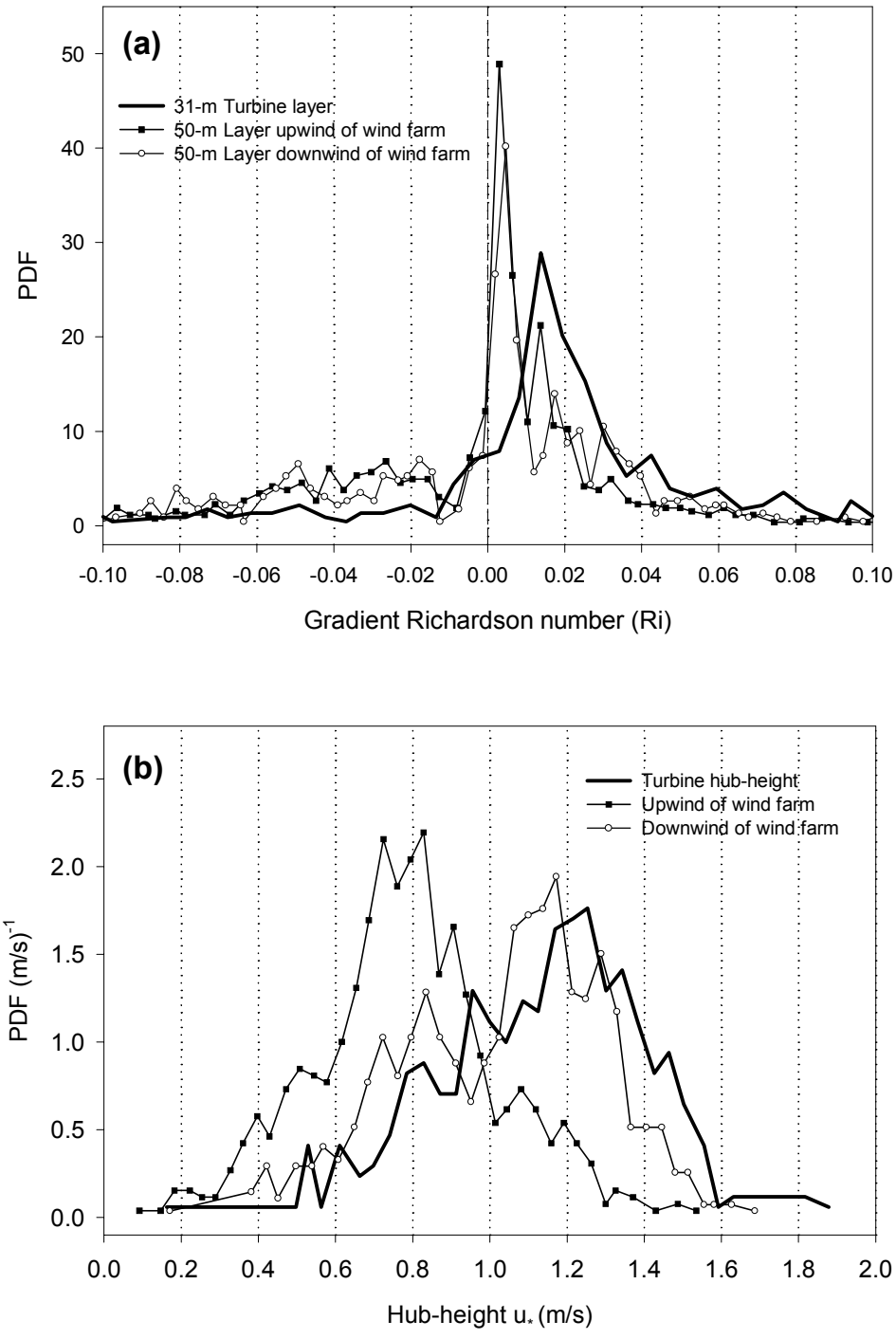

Figure 5. Probability distirbutions of (a) gradient Richardson numbers and (b) hub-height u_* or friction velocity

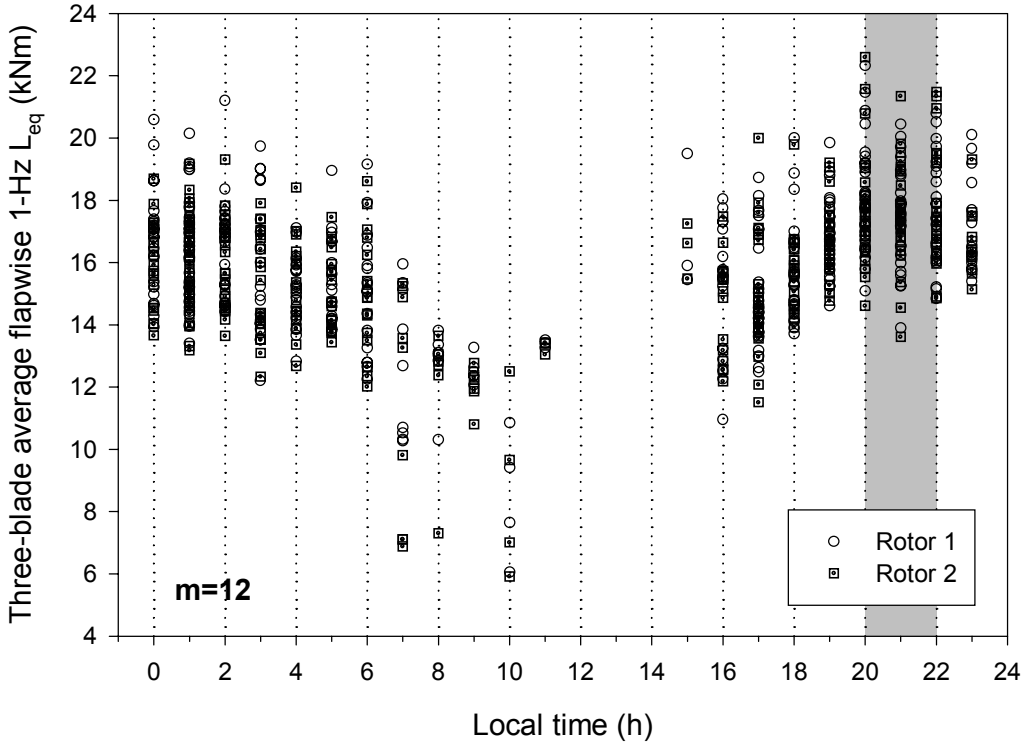

Figure 6. Diurnal variation of 1-Hz L_{eq} for Rotors 1 and 2

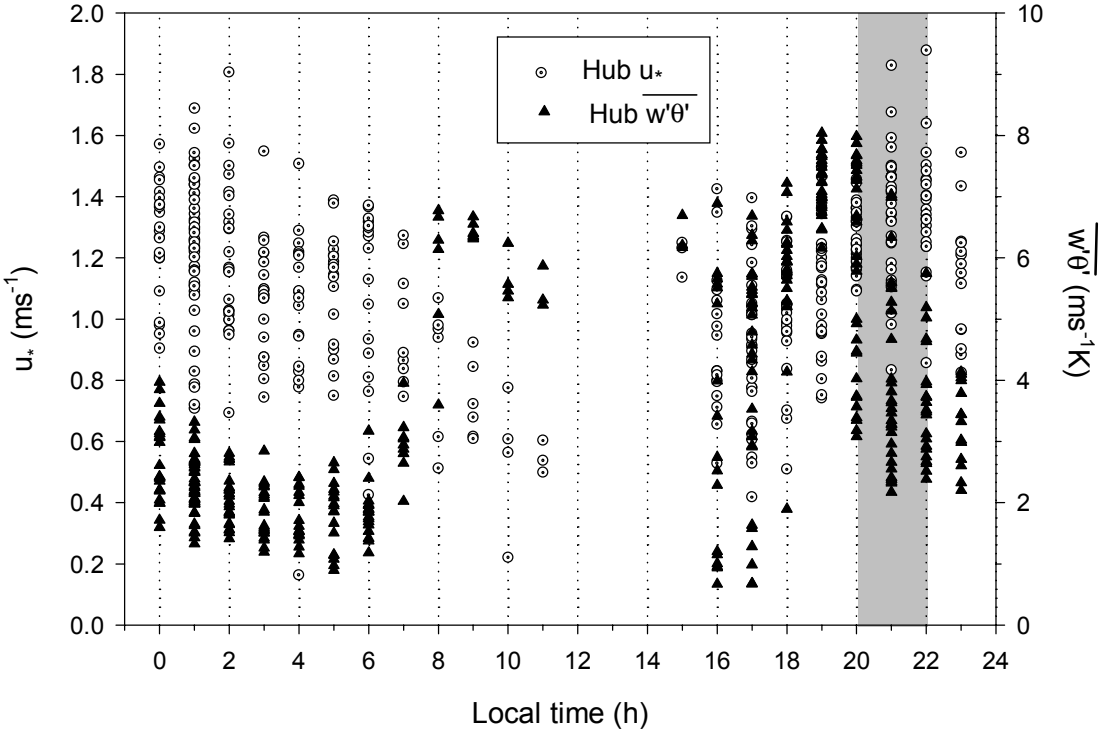

Figure 7. Diurnal variation of hub u_* and vertical temperature flux, $\overline{w'\theta'}$

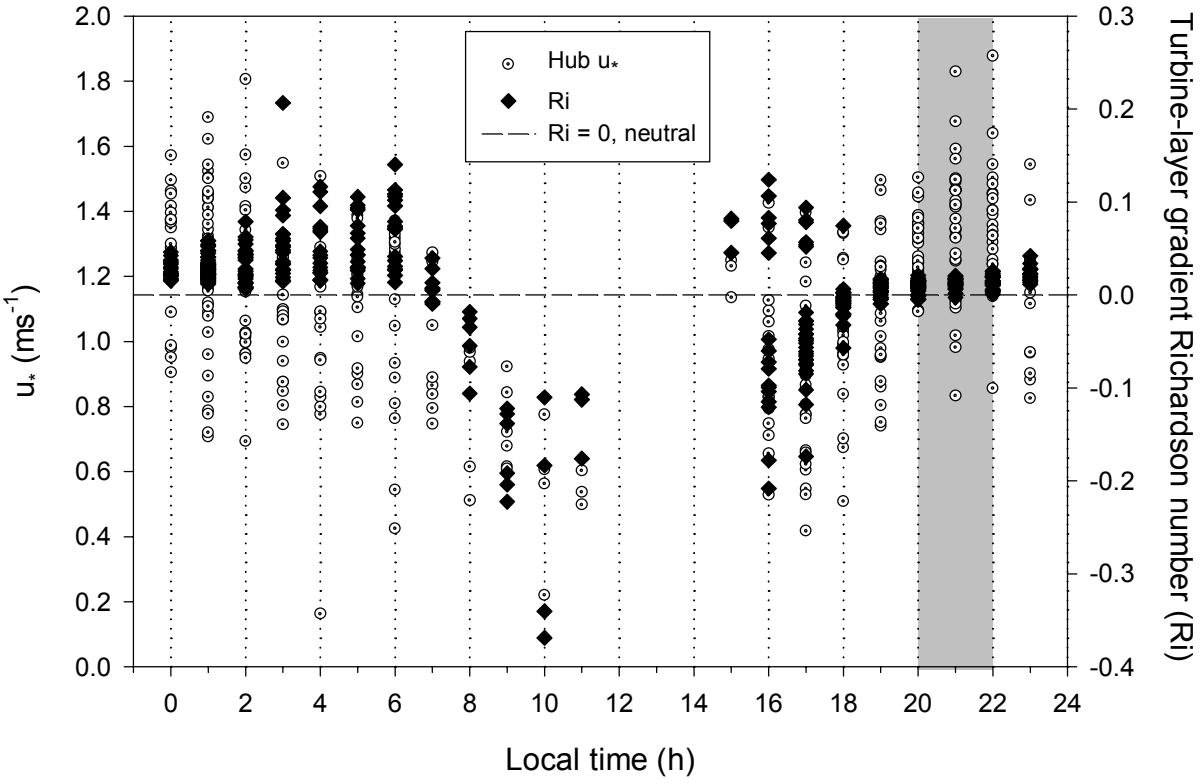

Figure 8. Diurnal variation of Richardson number and hub-height u_*